Mass and force-constant disorder in the rocksalt $Cd_{1-x} Zn_x O$ alloy: A Raman scattering study

Ramon Cuscó ⬤

GEO3BCN-CSIC, Consejo Superior de Investigaciones Científicas, Lluís Solé i Sabarís s.n., 08028 Barcelona, Spain

Javier Yeste ⬤ and Vicente Muñoz-Sanjosé ⬤

Dept. Física Aplicada i Electromagnetisme, Universitat de València, Dr. Moliner 50, València, 46100 Burjassot, Spain

We present a Raman scattering study of rocksalt $Cd_{1-x}Zn_xO$ alloys in the compositional range between $x = 0$ and $x = 0.1$. We use the sharp feature in the second-order Raman spectra associated with the transverse acoustic (TA) modes at the L point to monitor the effect of alloy disorder on the phonon lifetime. The 2TA(L) peak shows a substantial broadening as the Zn content is increased up to 10%. The rate of increase is significantly higher than that expected from cationic mass fluctuation as predicted by the mean-field coherent potential approximation. Excellent agreement with the experiment is achieved by including the effect of the force-constant fluctuations using the itinerant coherent potential approximation, demonstrating the significant role of the force-constant disorder in limiting the phonon lifetime in the $Cd_{1-x}Zn_xO$ alloys.

I. INTRODUCTION

CdO, a semiconductor that crystallizes in the rocksalt structure, has recently emerged among the transparent conducting oxides as a unique plasmonic material for mid-infrared applications [1]. CdO exhibits exceptionally low optical losses due to its low effective mass, high electron concentration and high electron mobility [1–3]. The sharp epsilon-near-zero resonance can be tuned over the entire mid-infrared (IR) range while maintaining high quality factors by using aliovalent dopants of similar atomic radii that minimize lattice strain [4]. The rocksalt $Cd_{1-x}Zn_xO$ alloy offers an alternative route to modulating the plasma frequency while enhancing the transparency in the visible range [5]. A simultaneous increase in electron density and electron mobility has been reported upon Zn incorporation up to 10% [5]. Surface plasmon polariton resonances with good quality factors have recently been reported in $Cd_{1-x}Zn_xO$ layers deposited on GaAs, opening the door to the integration of the plasmonic material with GaAs-based mid-IR optoelectronic technology [6].

The development of advanced applications will require a good knowledge of the basic physical properties of the $Cd_{1-x}Zn_xO$ alloy. Raman scattering is widely used to investigate phonons in semiconductors and to characterize their crystal quality. However, its use in rocksalt structures is severely limited because the first-order Raman scattering is forbidden by symmetry [7,8]. Nevertheless, the second-order Raman spectra display a number of sharp features associated with critical points in the phonon dispersion that have been used to extract information about the phonon lifetime [8]. When the lighter Zn atom is incorporated to the lattice, the coherence length of the phonons is reduced due to elastic scattering by the fluctuations in the alloy, which results in a disorder-induced intrinsic broadening of the phonons.

In addition to the high technological interest of $Cd_{1-x}Zn_xO$ for plasmonic applications, this compound is an ideal platform for the study of the effects of alloy disorder. At low Zn contents ($x \lesssim 0.3$) [9], $Cd_{1-x}Zn_xO$ has a relatively simple crystal structure formed by two interpenetrating face-centered-cubic (fcc) lattices, which lends itself to analytical lattice-dynamics calculations. There is also a large mass difference between the two cations of the alloy ($M_{Cd} = 112.4$ u vs. $M_{Zn} = 65.4$ u), which must lead to a strong scattering regime by mass defects and hence to a significant phonon broadening. Furthermore, the ionic radius of Cd is notably larger than that of Zn (0.95 vs 0.74 Å) [10], which will have an impact on the force constants between these isovalent cations. In fact, *ab initio* lattice-dynamics calculations [11] revealed a transverse-optical frequency of fcc ZnO that is somewhat lower than that of CdO, despite the much lighter cation mass, thus suggesting significant differences in their respective force constants.

The problem of disorder-induced phonon broadening has been extensively investigated in semiconductors with isotopic disorder [12–16]. Most studies are based on the lowest-order perturbation-theory calculation of the phonon self-energy. The disorder-induced scattering rate, which corresponds to the imaginary part of the self-energy, was calculated by Tamura and is proportional to the mass variance and to the phonon density of states (PDOS) [17]. For systems with large mass variance, such a lowest-order approach proved to be insufficient, and a treatment based on the coherent potential approximation (CPA) provided a better description of the experiments [15,18]. The CPA is a multiple-scattering, mean-field theory in which the disordered crystal is replaced by a self-consistent effective medium where the average scattering from each cell vanishes [19]. In the CPA, only the effects of the mass fluctuations (on-site disorder) are susceptible to calculation, and therefore CPA cannot account for the disorder in two-site quantities such as the force constants. While this is a good approximation for the case of isotopic disorder, it

may not be appropriate to treat disorder in alloys where the different cation species give rise to significant fluctuations in the force-constant environment. Force-constant disorder was included in a mean-field theory by using the itinerant CPA (ICPA) formulation in the augmented space of all possible configurations [20,21]. Recently, *ab initio* supercell phonon-unfolding simulations have shown good agreement with ICPA when the statistical distribution of the force constants is not very wide [22], as is probably the case in the relatively diluted alloys studied in this work. Furthermore, it was also revealed that, generally, ICPA properly accounts for the off-diagonal disorder associated with the averaged interspecies force constant fluctuations [22].

In this work, we present a Raman-scattering study of the disorder-induced effects on the phonons of the $Cd_{1-x}Zn_xO$ alloy for Zn fractions up to 0.1, well within the rocksalt structure regime [9]. We analyze the broadening of the prominent two transverse acoustic [2TA(L)] sharp feature of the second-order spectra with increasing Zn fraction. The effects of mass and force-constant disorder are discussed, and the predictions of the CPA and ICPA models are compared with the Raman spectra. The paper is organized as follows: In Sec. II we describe the details of the sample growth, the experimental conditions of the Raman measurements, and specific aspects of the *ab initio* calculations. In Sec. III we discuss the general features of the Raman spectra and the contributions of the two-phonon density of states (2PDOS) and charge density fluctuations (CDF) to the Raman profile observed in the experiments. A brief outline of the CPA model for the mass disorder and a comparison of the results with the Raman spectra is given in Sec. IV. Section V provides an overview of the main ideas of the ICPA model and deals with the extension of the fcc elastic model to next-nearest-neighbors (NNN) and the intra- and interspecies force-constant determination in the cation sublattice. Finally, the results of the ICPA model are compared with the Raman spectra.

II. EXPERIMENT

Single crystal $Cd_{1-x}Zn_xO$ epilayers with $x = 0.01, 0.025, 0.05, 0.075,$ and 0.1 were grown by metal-organic vapor-phase epitaxy on r-plane sapphire substrates. The epilayers had a thickness of $\sim$500 nm. Tertiary butanol and dimethylcadmium were used as precursors in a a reactor equipped with two independent gas inlets. The sample was kept at $304\,^\circ$C on a radio-frequency heated graphite susceptor.

Raman spectra were excited using the 514.5-nm line of an Ar^+ laser in backscattering geometry from a c surface. The scattered light was analyzed using a Jobin-Yvon T64000 spectrometer equipped with a liquid N_2 (LN_2) cooled charge-coupled detector. The measurements were performed at 80 K using a TBT-AirLiquide LN_2 cryostat.

Ab initio calculations in the virtual crystal approximation (VCA) were carried out to obtain phonon frequencies, PDOS, and force constants from the alchemical mixed pseudopotential approach provided in the ABINIT package [23]. Since alchemical calculations are only implemented with norm-conserving pseudopotentials we had to use the revised Perdew-Burke-Ernzerhof exchange-correlation functionals for the (Cd,Zn) pseudoatom instead of the ultrasoft

pseudopotentials we employed in our previous work on CdO [8]. Density functional perturbation theory calculations were performed in the framework of local density approximation. An energy cutoff of 60 hartree and a $6 \times 6 \times 6$ Monkhorst-Pack k-point sampling were used in the calculations.

III. THE RAMAN SPECTRA OF $Cd_{1-x}Zn_xO$

Because each atom of the lattice is a center of inversion, first-order Raman scattering is forbidden by symmetry in the rocksalt structure [7]. The second-order Raman spectrum of CdO was studied in detail in a previous publication [8], revealing a number of sharp features correlated with the overtone PDOS. These were observed on a broad background arising from overdamped oscillations of the high-density free-electron plasma [8,24]. In the acoustic-overtone spectral region, a sharp peak corresponding to the 2TA(L) mode stands out against a relatively low background and separated from the sapphire modes. We will focus on this isolated peak to study the effect of mass and force-constant disorder on the phonon linewidth. In Fig. 1 we illustrate the relative contributions of phonon overtones and plasma oscillations to the Raman spectra.

Neglecting possible scattering efficiency enhancements due to electron-photon and electron-phonon matrix elements, the second-order Raman spectrum profile would be given by the convolution of the individual overtone line shape and the overtone PDOS. It turns out, however, that the overtone scattering efficiency is notably enhanced at the edge of the Brillouin zone, which results in a 2TA(L) feature that is narrower than the straightforward convolution with the overtone PDOS. We have included an enhancement factor around the critical points L, X, and $\Delta \sim \frac{2}{3}\overline{\Gamma\text{-}X}$, which give rise to the peaks in the overtone PDOS (see Ref. [8]), to account for this effect. The enhancement factor is given by $\Xi(\omega) = 1 + a_L \mathscr{L}(\omega_{2TA(L)}) + a_X \mathscr{L}(\omega_{2LA(X)}) + a_\Delta \mathscr{L}(\omega_{2LA(\Delta)})$, where $\mathscr{L}(\omega_0)$ is a Lorentzian distribution of full width at half maximum (FWHM) = 6 cm^{-1} around ω_0. The coefficients $a_L = 4$, $a_X = 6$, and $a_\Delta = 13$ were adjusted for the case of pure CdO to obtain a good agreement with the measured Raman spectrum. The anharmonic decay and background impurity scattering were taken into account by considering an intrinsic 2TA(L) phonon linewidth of FWHM=10 cm^{-1}. This value is consistent with the results of our previous temperature dependence study of Raman scattering in CdO [8]. For the alloy, the 2TA(L) phonon line shape obtained from the ICPA calculations (Sec. V A) was used. The same enhancement factor $\Xi(\omega)$ was applied in all alloy compositions. Convolving the intrinsic phonon line shape with the enhanced overtone profile yields the second-order Raman spectrum, which was then superimposed on the CDF contribution [8,24] to obtain calculated line shapes (calc.) in good overall agreement with the experimental Raman spectra.

The Raman spectra of $Cd_{1-x}Zn_xO$ samples at 80 K are displayed in Fig. 2 for Zn fractions up to 10%. The 2TA(L) mode can be observed in all spectra and it broadens rapidly and decreases in intensity with increasing Zn composition. An extremely weak band at about 230 cm^{-1} is also observed. The origin of this feature, whose frequency and width remain unaltered as the Zn content is increased up to 10%, is
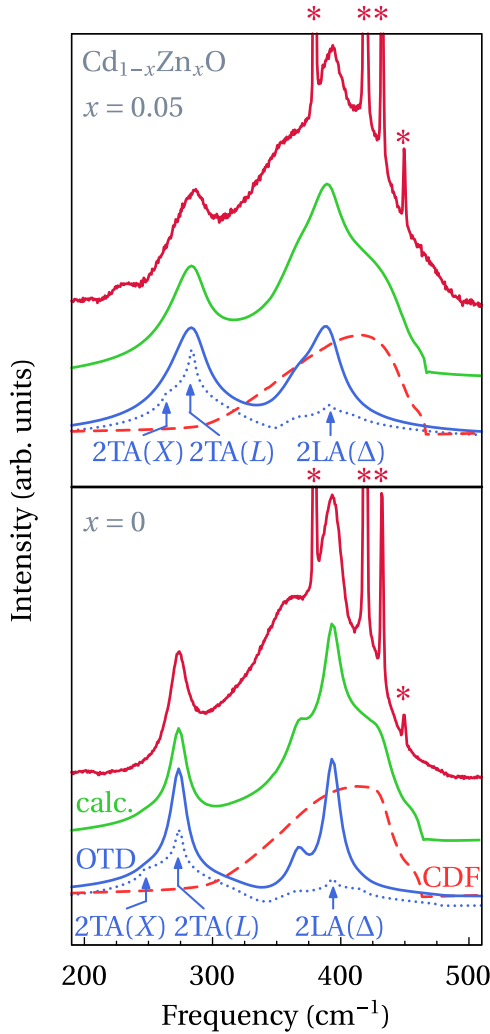
FIG. 1. Raman spectra of CdO and $Cd_{0.95}Zn_{0.05}O$ at 80 K (top red curves in each panel) and the different contributions in the spectral region of the acoustic overtones. The dotted line is the phonon-overtone density of states. The peaks corresponding to the critical points in the PDOS (L, X, and $\Delta \sim \frac{2}{3}\overline{\Gamma\text{-}X}$) are indicated by the arrows. The dashed line represents the the charge-density-fluctuation (CDF) scattering and the blue curve corresponds to the overtone contribution (OTD) to the Raman spectra. The green curve (calc) is the calculated spectrum obtained by adding these two contributions. The peaks marked with asterisks correspond to the sapphire substrate.

not clear. We speculate that it could be due to a sapphire second-order band or to the sapphire/$Cd_{1-x}Zn_xO$ interface, since it appears more clearly in the layers with higher Zn content, which have an increased transparency to the excitation light.

As discussed in our previous work [8], the high electron density present in these samples (on the order of 3×10^{20} cm^{-3}) gives rise to a broad background due to overdamped plasma oscillations and it opens the band gap due to the Burstein-Moss effect. As the Zn fraction increases, the band gap further blueshifts and the peaks from the sapphire substrate gain intensity as the layer becomes less light-absorbing at the excitation wavelength. Both effects interfere with the observation of the 2LA(Δ) line
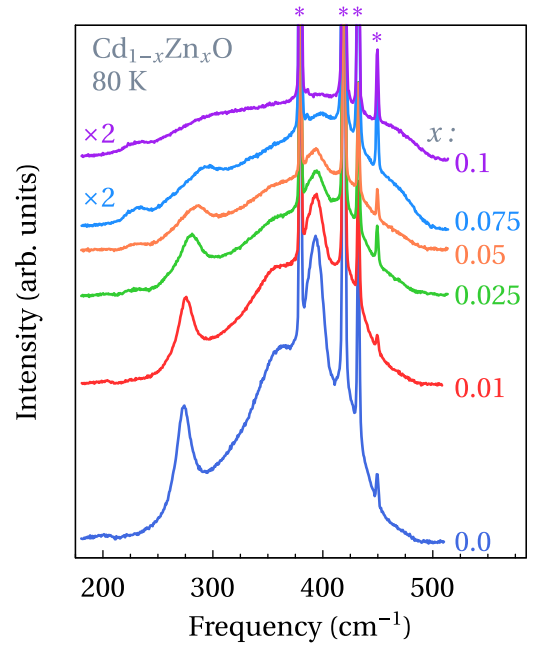

FIG. 2. Raman spectra of $Cd_{1-x}Zn_xO$ alloy for increasing Zn fraction at 80 K in the spectral region of the acoustic overtones. The peaks marked with asterisks correspond to the sapphire substrate.

shape, whereas the 2TA(L) mode is essentially free of these drawbacks.

IV. MASS DISORDER

A. Theory: The CPA model

Given the large difference in cationic masses, phonon scattering by mass fluctuations is expected to play an important role in the $Cd_{1-x}Zn_xO$ alloy, where mass disorder is limited to the cation sublattice. We start therefore by considering only the effect of cationic mass fluctuation.

The CPA model developed by Taylor [19] has been widely used to study the effects of mass disorder in isotopically disordered crystals [12,13,18,25] and in mixed-crystal systems [26,27]. Since we will be monitoring the alloy disorder using the sharp 2TA(L) feature, we focus on the acoustic modes of the alloy. These mainly involve the motion of the cation atoms, as illustrated by the CdO phonon density of states projected on the Cd sites [8]. We therefore restrict our analysis of the acoustic modes to the cationic sublattice.

The CPA considers an effective medium with a mass defect δM relative to the average mass $\langle M \rangle$ of the VCA alloy, which is characterized by a frequency-dependent complex self-energy $\tilde{\varepsilon}(\omega)$. The self-energy is self-consistently evaluated by imposing that the average scattering from a single site vanishes. Then, $\tilde{\varepsilon}(\omega)$ is determined from the relation [28]

$$\langle M \rangle \tilde{\varepsilon}(\omega) = \frac{x(1-x)(\delta M)^2 \omega^2 \mathscr{G}(\omega^2)}{1 + [(1+2x)\delta M + \langle M \rangle \tilde{\varepsilon}(\omega)]\omega^2 \mathscr{G}(\omega^2)}, \quad (1)$$

where

$$\mathscr{G}(\omega^2) = \frac{1}{\langle M \rangle} \int_0^\infty \frac{g_{VCA}(\eta) d\eta}{\omega^2 [1 - \tilde{\varepsilon}(\omega)] - \eta^2} \quad (2)$$

is the site Green's function and $g_{VCA}(\omega)$ is the PDOS of the virtual crystal. The phonon self-energy produces a frequency shift to

$$\omega_{CPA} = \omega_{VCA}[1 - \text{Re}\{\tilde{\varepsilon}(\omega_{CPA})\}]^{-1/2} \tag{3}$$

and a FWHM broadening

$$\Gamma_{CPA} = -\omega_{CPA}\text{Im}\{\tilde{\varepsilon}(\omega_{CPA})\}. \tag{4}$$

Using the PDOS projected on the cation sites as obtained from ABINIT VCA calculations, we evaluate Eq. (1) iteratively until convergence on $\tilde{\varepsilon}(\omega)$ is reached. It must be stressed that only mass fluctuations (on-site or diagonal disorder) can be addressed within the CPA formalism.

The second-order Raman spectra closely follows the overtone PDOS, which is also broadened by disorder according to [12]

$$\rho_{OT}(2\omega)$$

$$= -\frac{2}{\pi\omega}\int_0^\infty g_{VCA}(\eta)$$

$$\times \frac{\omega^2\text{Im}\{\tilde{\varepsilon}(\omega)\}}{[\omega^2(1 - \text{Re}\{\tilde{\varepsilon}(\omega)\}) - \eta^2]^2 + \omega^4\text{Im}\{\tilde{\varepsilon}(\omega)\}^2}\eta^2 d\eta. \tag{5}$$

The final line shape is obtained from the convolution of a Lorentzian line shape of FWHM = $2\Gamma_{CPA}$, corresponding to the second-order phonon, with the overtone scattering-efficiency profile

$$\text{OTD}(\omega) = \Xi(\omega)\rho_{OT}(\omega)[n_{BE}(\omega/2, T) + 1]^2, \tag{6}$$

where $n_{BE}(\omega)$ is the Bose-Einstein occupation factor.

B. Results

Figure 3 displays the 2TA(L) Raman peaks at 80 K for Zn concentrations between 0 and 0.1. The background of the spectra was carefully subtracted by taking into account the elbowlike profile of the CDF contribution in this frequency range and adjusting its slope to match the Raman spectra. The experimental results are compared with the predictions of the CPA model, displayed as solid lines. The agreement between theory and experiment is excellent for the pure CdO crystal and for the $x = 0.01$ alloy, but as the Zn concentration increases, striking discrepancies become apparent. On the one hand, the theoretical line shapes show very little frequency upshift with increasing Zn content. This results from an important underestimation of the phonon frequencies by the VCA *ab initio* calculations, which are based on a crude mixing of pseudopotentials that may not account properly for the large difference in cationic radii [29]. The small frequency increase with Zn composition given by the VCA model is nearly compensated by the frequency downshift due to mass disorder [Eq. (3)]. On the other hand, although the CPA model does predict a gradual increase of FWHM with increasing Zn composition, its magnitude is significantly lower than that observed in the Raman spectra. These results indicate that mass disorder alone cannot explain the experimental observations. On account of the large difference in cationic radii, it is necessary to take into account force-constant fluctuations in the treatment of the alloy disorder.
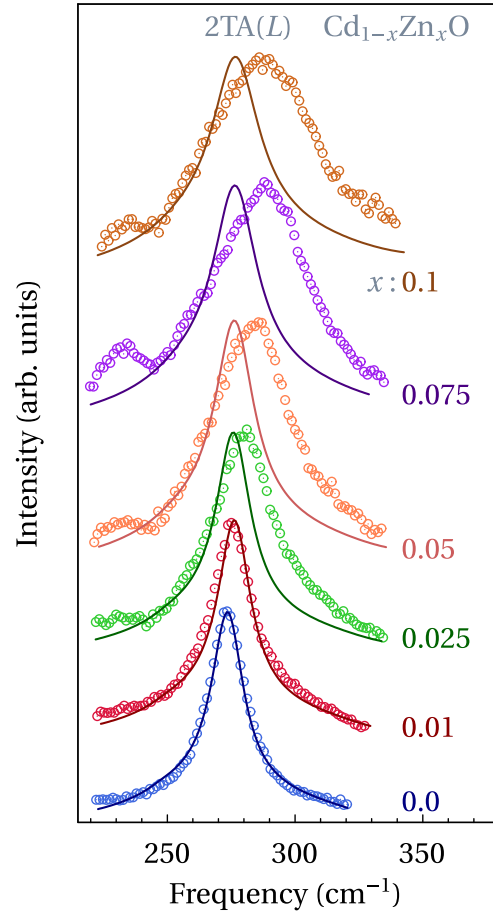

FIG. 3. Raman spectra of the 2TA(L) peak at 80 K of $Cd_{1-x}Zn_xO$ for $0 < x < 0.1$ after background subtraction (circles). The solid lines are the mass-disorder broadened line shapes as predicted by the CPA model.

V. MASS- AND FORCE-CONSTANT-DISORDER

A. Theory: the ICPA model

Including force-constant changes in a CPA approach is a nontrivial problem because the sum of the force constants $\Phi_{ll'}$ between a site l and its neighbors must verify Newton's third law, i.e., $\sum_{l'} \Phi_{ll'} = 0$. Thus, a fluctuation on site l affects the neighboring sites leading to environmental disorder. A self-consistent cluster theory was formulated in the augmented space of all possible random disorder configurations by Kaplan *et al.* [20] and later applied to face centered cubic (fcc) binary alloys with nearest-neighbor (NN) interaction by Ghosh *et al.* [21]. In this framework, when a phonon interacts with a fluctuation at site l, it also scatters from its neighbors via changes in the force constants. Therefore, the scattering by fluctuations on all of the neighboring sites has to be included, which eventually leads the scattering to extend over the entire crystal. The coherent potential for a single fluctuation state is self-consistently determined taking into account the itineration of the fluctuation in the average medium and defines the ICPA. Multiple uncorrelated fluctuations are self-consistently incorporated in the itinerator operator $\mathbf{F}(\mathbf{q})$ by considering a conditional propagator $\mathbf{G}^{(0)}$ that includes those scatterings that neither start nor end at the site considered [21].

Since the scattering may have started at any site, the theory is translationally invariant and the phonon self-energy $\Sigma(\mathbf{q})$ can be determined in $\mathbf{q}$ space by Fourier transforms on the fluctuation sites. The configuration-averaged Green's function is then given by $\langle\langle\mathbf{G}(\mathbf{q})\rangle\rangle = [\mathbf{G}_{\mathrm{VCA}}(\mathbf{q})^{-1} - \Sigma(\mathbf{q})]^{-1}$, where $\mathbf{G}_{\mathrm{VCA}}(\mathbf{q})$ is the Green's function of the average VCA crystal. The partition of the augmented space into the average configuration space and the rest of fluctuation states greatly simplifies the algebra of operator inversion [21]. The ICPA spectral function, which is proportional to the Raman cross section, is defined by the imaginary part of the $\mathbf{q}$-space Green's function. Explicit expressions for the itinerator operators are given for a fcc system with NN interaction in Ref. [21]. Unfortunately, the ICPA model becomes very complicated and essentially unfeasible for systems more complex than binary alloys, and a full description of the $Cd_{1-x}Zn_xO$ lattice dynamics is out of the question. Nevertheless, as shown below, the ICPA can be applied to the cationic sublattice to gain insight into the effect of disorder on the acoustic phonons as described in Sec. V B.

The numerical integrations involved in the Fourier transforms were carried out using a set of 408 special points in the irreducible 1/48th wedge of the Brillouin zone [30]. The VCA propagator was used as an initial guess for $\mathbf{G}^{(0)}$ to calculate $\mathbf{F}(\mathbf{q})$ and $\Sigma(\mathbf{q})$ at a frequency close to the spectral density peak. The self-energy $\Sigma(\mathbf{q})$ in turn determines $\langle\langle\mathbf{G}(\mathbf{q})\rangle\rangle$, and from this configuration-averaged propagator a new $\mathbf{G}^{(0)}$ is obtained. The latter is used to recalculate $\mathbf{F}(\mathbf{q})$ and the process is iterated until self-consistency is reached. A linear mixing scheme $\mathbf{G}^{(0)} = \alpha\mathbf{G}_{\mathrm{out}}^{(0)} + (1-\alpha)\mathbf{G}_{\mathrm{in}}^{(0)}$ with $\alpha = 0.6$ was used to accelerate convergence. The configuration-averaged propagator obtained at each frequency was used as the initial guess for $\mathbf{G}^{(0)}$ at the adjacent frequency in the spectral density calculation.

B. VCA model up to next-nearest neighbors for the acoustic phonons

Owing to the large mass difference between cations and anions in the $Cd_{1-x}Zn_xO$ alloy, the lower frequency modes mainly involve the heavier cations. This is illustrated by the phonon density of states projected onto the O sites, which is negligible in the acoustic frequency range [8]. Since the $Cd_{1-x}Zn_xO$ crystal consists of two interpenetrating fcc lattices, we consider only the fcc cation sublattice for describing the disorder effects on the $2TA(L)$ mode. For the determination of the intraspecies force-constant parameters we consider the interatomic interactions in a fictitious fcc lattice comprised of either Cd or Zn atoms. As illustrated in Fig. 4, where the results of the Cd sublattice calculation are compared with *ab initio* VCA calculations of CdO, it turns out that the NN interaction is insufficient to provide a reasonable description of the lattice dynamics, and NNN interactions are essential to achieve a good agreement with the acoustic phonon dispersion. The force-constant matrices for the NN and NNN interactions in the fcc system are of the form

$$\Phi_{(000),(\frac{a}{2}\frac{a}{2}0)}^{\mathrm{NN}} = \begin{pmatrix} a_1 & b_1 & 0 \\ b_1 & a_1 & 0 \\ 0 & 0 & g_1 \end{pmatrix},$$
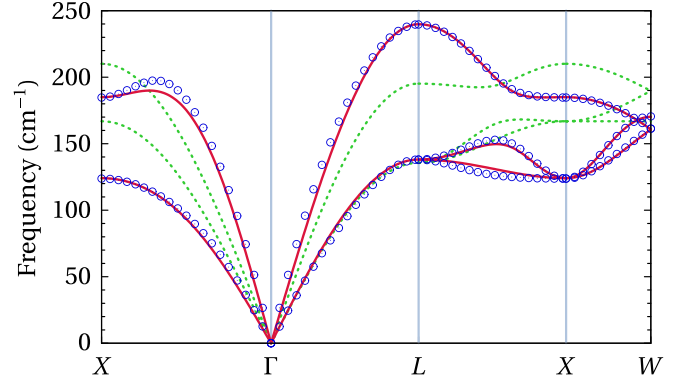

FIG. 4. Acoustic phonon dispersion of CdO along high-symmetry directions calculated in the NNN approximation of the cation sublattice (solid lines), compared to full-crystal *ab initio* calculations (circles). The dotted lines display the results of the NN approximation.

$$\Phi_{(000),(00a)}^{\mathrm{NNN}} = \begin{pmatrix} a_2 & 0 & 0 \\ 0 & a_2 & 0 \\ 0 & 0 & g_2 \end{pmatrix}, \tag{7}$$

and the matrices for the rest of the NN and NNN are generated by symmetry operations. Given the particularly simple form of the NNN interaction matrices, it is straightforward to generalize the NN expressions of the ICPA operators given in Ref. [21] to include NNN interactions. The ICPA operators thus become 57×57 complex matrices.

We adjust the parameters a_1, b_1, g_1, a_2, g_2 for the fcc lattices of Cd and Zn so that the diagonalization of their dynamical matrices reproduce the $TA(L)$ frequencies of the respective oxides and fit the TA and LA frequencies along high symmetry directions. Optimized parameters for Cd–Cd and Zn–Zn force constants are listed in Table I. Since the Zn atom is sizably smaller than the Cd atom, the average Cd-Cd distance in the alloy is lower than in pure CdO. Conversely, the Zn–Zn distance is higher in the alloy. Assuming a d^{-4} bond-length dependence of the force constants [31,32], the intraspecies Cd–Cd and Zn–Zn force constants in the alloy are scaled to

$$\Phi_{\mathrm{Cd-Cd}}^{\mathrm{alloy}} = \Phi_{\mathrm{Cd-Cd}}^{\mathrm{CdO}}\left(\frac{a_{\mathrm{CdO}}}{a_{\mathrm{CdZnO}}}\right)^4 \tag{8}$$

TABLE I. Lattice parameter of $Cd_{1-x}Zn_xO$ in the virtual crystal approximation and force-constant parameters in the cation sublattice optimized to reproduce the acoustic phonon dispersion of the alloy.

x	a (Å)	Force constants (dyn cm^{-1})				
		a_1	b_1	g_1	a_2	g_2
0.00	4.691	358.81	−537.50	35.83	−43.03	−569.37
0.01	4.688	358.14	−546.51	38.97	−44.19	−572.23
0.025	4.683	362.22	−520.26	27.10	−41.95	−558.86
0.05	4.675	367.04	−485.94	11.12	−39.41	−539.85
0.075	4.667	370.46	−472.66	2.27	−36.55	−531.20
0.10	4.658	370.66	−458.17	3.15	−38.16	−520.15
1.00	4.259	368.36	−246.86	0.90	−86.56	−368.98

and

$$\Phi_{\text{Zn-Zn}}^{\text{alloy}} = \Phi_{\text{Zn-Zn}}^{\text{ZnO}} \left(\frac{a_{\text{ZnO}}}{a_{\text{CdZnO}}} \right)^4, \tag{9}$$

where a_{CdO}, a_{ZnO}, and a_{CdZnO} are the lattice parameters of the CdO, ZnO, and CdZnO crystals, respectively. The lattice parameters for the alloys were obtained from ABINIT calculations and are listed in Table I.

For the determination of the interspecies Cd–Zn force constants we calculated the phonon dispersion in the alloy using the ABINIT alchemical approach. The resulting frequencies were aligned with the critical points of the Raman spectra and the NNN model was fitted to the high symmetry points in the same way that was carried out for the determination of Φ_{CdO} and Φ_{ZnO}. This procedure ensures that the NNN model reproduces the alloy frequencies observed in the Raman measurements. The interspecies force constants $\Phi_{\text{Cd-Zn}}$ are then obtained from the relation

$$\Phi_{\text{Cd}_{1-x}\text{Zn}_x\text{O}} = (1-x)^2 \Phi_{\text{Cd-Cd}} + x^2 \Phi_{\text{Zn-Zn}}$$
$$+ 2x(1-x)\Phi_{\text{Cd-Zn}}. \tag{10}$$

C. Results

The 2TA(L) line-shape simulations based on the ICPA model are compared with the Raman spectra in Fig. 5. The calculations are in excellent agreement with the Raman data. Since the phonon frequencies of the alloy used to evaluate the force constants in the NNN model of the cation sublattice were extracted from the Raman spectra, these simulations are not affected by the underestimation of the phonon frequencies by the VCA *ab initio* calculations. Therefore, the close frequency match with the Raman spectra was to be expected. Remarkably, the ICPA model also accounts very well for the line-shape broadening over the whole range of alloy compositions studied. As the Zn content of the alloy increases above 1%, the ICPA simulations reproduce the overall 2TA(L) line shape, in contrast with the much narrower and symmetrical line shapes predicted by the CPA model of mass disorder (see Fig. 3).

According to the ICPA model, the TA(L) phonon broadening due to alloy disorder is accompanied by a frequency downshift, which increases with Zn composition and reaches ~ 1.8 cm^{-1} for the $x = 0.1$ alloy. Therefore, the actual VCA frequencies are slightly higher than those inferred from the 2TA(L) feature of the Raman spectra. This is illustrated in Fig. 6, where we plot the dependence of the TA(L) frequency on the alloy composition. The increase of the TA(L) frequency with increasing Zn fraction derived from the Raman spectra is appreciably higher than the predictions of VCA *ab initio* calculations based on a straightforward combination of atomic pseudopotentials [23]. The shortcomings of this simple approach to accurately modeling the effects of the differences in chemical bonding are likely at the root of these discrepancies [29].

VI. SUMMARY AND CONCLUSIONS

We have investigated the Raman spectra of the Cd$_{1-x}$Zn$_x$O alloys for $0 < x < 0.1$ at $T = 80$ K. In this composition

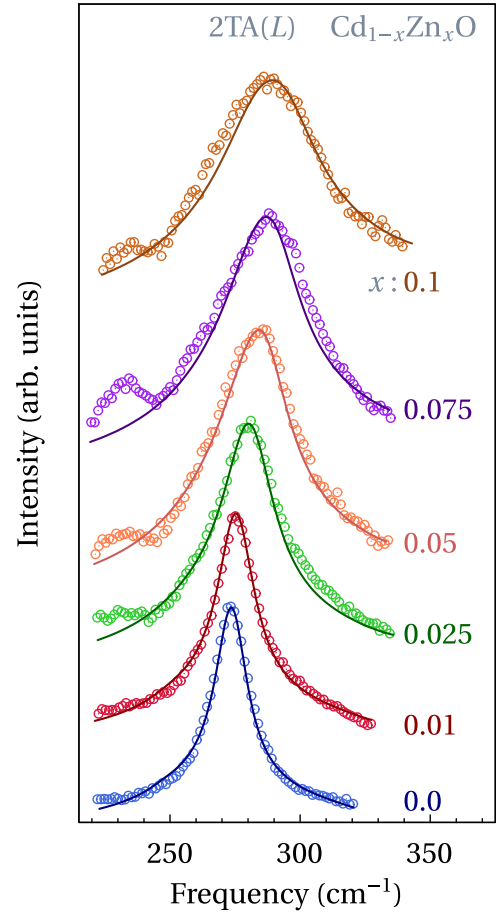FIG. 5. Line-shape simulations of the 2TA(L) peak of Cd$_{1-x}$Zn$_x$O for $0 < x < 0.1$ using the ICPA model (solid lines) compared with the 80 K Raman spectra (circles). For the sake of comparison, the spectra have been normalized to have the same peak intensity.
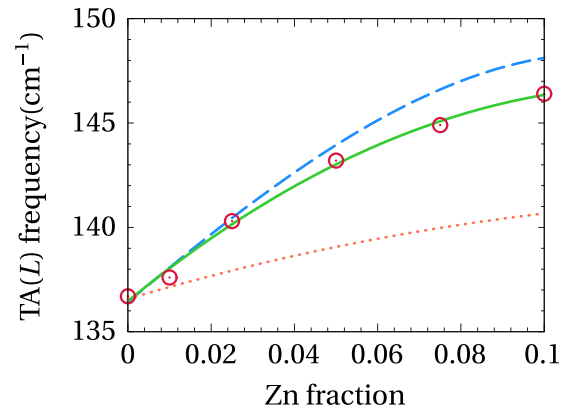

FIG. 6. Dependence of the TA(L) frequency on the alloy composition. Circles correspond to the halved frequency of the 2TA(L) feature in the Raman spectra (the solid line is a guide to the eye). The dashed line indicates the corresponding frequency of the NNN cation-sublattice model. The *ab initio* VCA calculations with averaged pseudopotentials are shown as a dotted line.

range, the alloys have a rocksalt structure and the first-order Raman spectrum is forbidden. The second-order Raman spectra show distinct features, most notably a relatively narrow 2TA(L) peak that evolves smoothly as the Zn fraction is increased and can be used to monitor the effects of alloy disorder. The frequency of the 2TA(L) feature increases with Zn fraction at a higher rate than predicted by VCA *ab initio* calculations based on average potentials. In spite of the large cationic mass difference, the conventional CPA model for mass disorder cannot account for the broadening of the 2TA(L) peak in the Raman spectra. These results suggest that the fluctuations in the force constants across the alloy play a prominent role in determining the phonon linewidth.

Mass and force-constant disorder effects are intertwined and cannot be separated. Force-constant perturbations affect not only the dynamical matrix of a defect site but also those of its neighbors. The ICPA mean-field theory accounts for the off-diagonal multiple scatterings and can be applied to the fcc cation sublattice of $Cd_{1-x}Zn_xO$ to describe disorder on the acoustic phonons of the alloy. An NNN elastic model of the cationic sublattice provides a good account of the acoustic phonon dispersion and it allows one to estimate the different pairwise force constants that can be used in the ICPA model. Excellent agreement between the 2TA(L) Raman lineshape simulations using the ICPA model and the Raman measurements is found for all the Zn fractions studied, thus highlighting the important role of force-constant disorder in the lattice dynamics of $Cd_{1-x}Zn_xO$. The force-constant variations stem from the disparity in ionic radii between Cd and Zn and the relaxation of the interatomic distances in the alloy.

[1] E. Sachet, C. T. Shelton, J. S. Harris, B. E. Gaddy, D. L. Irving, S. Curtarolo, B. F. Donovan, P. E. Hopkins, P. A. Sharma, A. L. Sharma, J. Ihlefeld, S. Franzen, and J.-P. Maria, Dysprosium-doped cadmium oxide as a gateway material for mid-infrared plasmonics, Nat. Mater. **14**, 414 (2015).

[2] P. H. Jefferson, S. A. Hatfield, T. D. Veal, P. D. C. King, C. F. McConville, J. Zúñiga-Pérez, and V. Muñoz-Sanjosé, Bandgap and effective mass of epitaxial cadmium oxide, Appl. Phys. Lett. **92**, 022101 (2008).

[3] S. K. Vasheghani Farahani, T. D. Veal, P. D. C. King, J. Zúñiga-Pérez, V. Muñoz Sanjosé, and C. F. McConville, Electron mobility in CdO films, J. Appl. Phys. **109**, 073712 (2011).

[4] E. L. Runnerstrom, K. P. Kelley, E. Sachet, C. T. Shelton, and J.-P. Maria, Epsilon-near-zero modes and surface plasmon resonance in fluorine-doped cadmium oxide thin films, ACS Photonics **4**, 1885 (2017).

[5] J. Tamayo-Arriola, A. Huerta-Barberà, M. M. Bajo, E. Muñoz, V. Muñoz-Sanjosé, and A. Hierro, Rocksalt CdZnO as a transparent conductive oxide, Appl. Phys. Lett. **113**, 222101 (2018).

[6] E. Martínez Castellano, J. Yeste, M. Abuin, M. d. C. Martínez-Tomás, O. Klymov, V. Muñoz Sanjosé, M. Montes-Bajo, and A. Hierro, Mid-IR surface plasmon polaritons in CdZnO thin films on GaAs, Appl. Surf. Sci. **608**, 155060 (2023).

[7] J. E. Potts, C. T. Walker, and I. R. Nair, Temperature dependence of second-order Raman scattering in potassium and rubidium halides, Phys. Rev. B **8**, 2756 (1973).

[8] R. Cuscó, J. Yeste, and V. Muñoz-Sanjosé, Temperature dependence of Raman scattering in CdO: Insights into phonon anharmonicity and plasmon excitations, Phys. Rev. B **107**, 125204 (2023).

[9] D. M. Detert, S. H. M. Lim, K. Tom, A. V. Luce, A. Anders, O. D. Dubon, K. M. Yu, and W. Walukiewicz, Crystal structure and properties of $Cd_xZn_{1-x}O$ alloys across the full composition range, Appl. Phys. Lett. **102**, 232103 (2013).

[10] R. D. Shannon, Revised effective ionic radii and systematic studies of interatomic distances in halides and chalcogenides, Acta Crystallogr. A **32**, 751 (1976).

[11] J. Serrano, A. H. Romero, F. J. Manjón, R. Lauck, M. Cardona, and A. Rubio, Pressure dependence of the lattice dynamics of ZnO: An *ab initio* approach, Phys. Rev. B **69**, 094306 (2004).

[12] H. D. Fuchs, C. H. Grein, C. Thomsen, M. Cardona, W. L. Hansen, E. E. Haller, and K. Itoh, Comparison of the phonon spectra of ^{70}Ge and natural Ge crystals: Effects of isotopic disorder, Phys. Rev. B **43**, 4835 (1991).

[13] K. C. Hass, M. A. Tamor, T. R. Anthony, and W. F. Banholzer, Lattice dynamics and Raman spectra of isotopically mixed diamond, Phys. Rev. B **45**, 7171 (1992).

[14] A. Göbel, T. Ruf, J. M. Zhang, R. Lauck, and M. Cardona, Phonons and fundamental gap in ZnSe: Effects of the isotopic composition, Phys. Rev. B **59**, 2749 (1999).

[15] S. Rohmfeld, M. Hundhausen, L. Ley, N. Schulze, and G. Pensl, Isotope-disorder-induced line broadening of phonons in the Raman spectra of SiC, Phys. Rev. Lett. **86**, 826 (2001).

[16] R. Cuscó, L. Artús, J. H. Edgar, S. Liu, G. Cassabois, and B. Gil, Isotopic effects on phonon anharmonicity in layered van der Waals crystals: A study of isotopically pure hexagonal boron nitride, Phys. Rev. B **97**, 155435 (2018).

[17] S. I. Tamura, Isotope scattering of large-wave-vector phonons in GaAs and InSb: Deformation-dipole and overlap-shell models, Phys. Rev. B **30**, 849 (1984).

[18] R. Cuscó, J. H. Edgar, S. Liu, J. Li, and L. Artús, Isotopic disorder: The prevailing mechanism in limiting the phonon lifetime in hexagonal BN, Phys. Rev. Lett. **124**, 167402 (2020).

[19] D. W. Taylor, Vibrational properties of imperfect crystals with large defect concentrations, Phys. Rev. **156**, 1017 (1967).

[20] T. Kaplan, P. L. Leath, L. J. Gray, and H. W. Diehl, Self-consistent cluster theory for systems with off-diagonal disorder, Phys. Rev. B **21**, 4230 (1980).

[21] S. Ghosh, P. L. Leath, and M. H. Cohen, Phonons in random alloys: The itinerant coherent-potential approximation, Phys. Rev. B **66**, 214206 (2002).

[22] S. Mu, R. J. Olsen, B. Dutta, L. Lindsay, G. D. Samolyuk, T. Berlijn, E. D. Specht, K. Jin, H. Bei, T. Hickel, B. C. Larson, and G. M. Stocks, Unfolding the complexity of phonon quasiparticle physics in disordered materials, npj Comput. Mater. **6**, 4 (2020).

[23] ABINIT is a common project of the Université Catholique de Louvain, Corning Incorporated, and other contributors (http://www.abinit.org). X. Gonze, J.-M. Beuken, R. Caracas, F. Detraux, M. Fuchs, G.-M. Rignanese, L. Sindic, M. Verstraete, G. Zerah, F. Jollet, M. Torrent, A. Roy, M. Mikami, P. Ghosez, J.-Y. Raty, and D. C. Allan, Comput. Mater. Sci. **25**, 478 (2002).

[24] R. Cuscó, J. Yeste, and V. Muñoz-Sanjosé, Erratum: Temperature dependence of Raman scattering in CdO: Insights into phonon anharmonicity and plasmon excitations, Phys. Rev. B **107**, 239902(E) (2023).

[25] H. D. Fuchs, P. Etchegoin, M. Cardona, K. Itoh, and E. E. Haller, Vibrational band modes in germanium: Isotopic disorder-induced Raman scattering, Phys. Rev. Lett. **70**, 1715 (1993).

[26] P. N. Sen and W. M. Hartmann, Coherent-potential approximation for the lattice vibrations of mixed diatomic systems, Phys. Rev. B **9**, 367 (1974).

[27] J. R. Gregg and C. W. Myles, Vibrational band modes in germanium: Isotopic disorder-induced Raman scattering, J. Phys. Chem. Solids **46**, 1305 (1985).

[28] H. Ehrenreich and L. M. Schwartz, *Solid State Physics* (Academic, New York, 1976), Vol. 31.

[29] N. J. Ramer and A. M. Rappe, Virtual-crystal approximation that works: Locating a compositional phase boundary in $PbZr_{1-x}Ti_xO_3$, Phys. Rev. B **62**, R743(R) (2000).

[30] D. J. Chadi and M. L. Cohen, Special points in the Brillouin zone, Phys. Rev. B **8**, 5747 (1973).

[31] W. A. Harrison, *Electronic Structure and the Properties of Solids. The Physics of the Chemical Bond* (Dover, New York, 1989).

[32] D. L. Crittenden, Simple, near-universal relationships between bond lengths, strengths, and anharmonicities, AIP Adv. **13**, 115323 (2023).